國 立 交 通 大 學

電信工程學系

碩 士 論 文

微型髮夾式諧振器並聯開路殘段實現
具有高頻寬截止帶雙頻帶通濾波器

Compact Hairpin Resonator Shunt Open Stub Bandpass Filters with Dual-Band Response and Wide Upper Stopband

研究生：謝秉岳

指導教授：郭仁財教授

中 華 民 國 九十八 年 八 月

微型髮夾式諧振器並聯開路殘段實現具有高頻寬截止帶雙頻帶通濾波器

Compact Hairpin Resonator Shunt Open Stub Bandpass Filters with Dual-Band Response and Wide Upper Stopband

研究生：謝秉岳 **Student:Ping-Yueh Hsieh**

指導教授：郭仁財 博士 **Advisor:Dr. Jen-Tsai Kuo**

國立交通大學

電信工程學系

碩士論文

A Thesis
Submitted to Department of Communication Engineering
College of Electrical and Computer Engineering
National Chiao Tung University
in Partial Fulfillment of the Requirements
for the Degree of
Master of Science
in
Communication Engineering
June 2009
Hsinchu, Taiwan, Republic of China

中華民國九十八年八月

微型髮夾式諧振器並聯開路殘段實現
具有高頻寬截止帶雙頻帶通濾波器

研 究 生：謝 秉 岳　　指 導 教 授：郭 仁 財　博 士

國立交通大學電信工程學系

摘要

本論文提出一微型化髮夾式並聯開路殘段諧振器去設計雙頻帶暨寬截止帶帶通濾波器，其中一開路殘段並聯於中間，而另外兩段則對稱地並聯在諧振器的兩側。利用調整開路殘段的阻抗及長度和並聯的位置使所有的諧振器皆有相同的兩個操作頻率，但是彼此的高階諧振頻率會互相錯開。為了增加壓抑的程度進而拓寬高頻截止帶，由並聯的架構和耦合線段所產生的傳輸零點來消除存餘的高階諧波。五階濾波器的量測結果顯示小於 28dB 的截止頻帶可以拓展到六倍的基頻頻率。而量測的結果與模擬結果吻合。

Compact Hairpin Resonator Shunt Open Stub Bandpass Filters with Dual-Band Response and Wide Upper Stopband

Student: Ping-Yueh Hsieh

Advisor: Dr. Jen-Tsai Kuo

Department of Communication Engineering

National Chiao Tung University

Abstract

Compact bandpass filters are devised with a dual-passband response and a wide upper stopband based on hairpin resonators with three shunt open stubs. One stub is tapped at the center and two are allocated on both sides symmetrically. By adjusting the stub lengths, all resonators are designed to have two identical leading resonant frequencies but different higher-order ones. To enhance the rejection level and extend the upper stopband, the transmission zeros created by the tap structures and the coupled-line stage are used to eliminate the remaining leading unwanted peaks. Measured results show that the fifth-order filter has a rejection level below 30 dB can be extended to six times the first frequency. Good agreement between measured and simulation is obtained.

Acknowledgement

誌謝

能夠完成本篇論文首先要感謝的是一直指導並細心糾正我錯誤的郭仁財教授，郭老師不僅在研究上給予我很多很多建議，讓我在研究的瓶頸時總能看到一絲曙光，而且在為人處世上，郭老師的認真謹慎更是值得我學習的地方，我要在此致上十二萬分的感謝，郭老師，謝謝您！同時也要感謝百忙之中抽空來為我的論文作出指導的陳俊雄教授、林祐生教授以及鐘世忠教授，謝謝！

還有實驗室的成員，多得你們的陪伴，使得我研究生涯很多采多姿。在我有很多問題時總是可以幫我解答的逸群學長，除了要管理整個實驗室的大大小小事之外還要做研究，學長的勤奮也是我要學習的典範。還有上一屆的學長姊，聰明的宇峯，無厘頭的承軒，搞笑的欣穎，認真的慧萍，多謝你們陪我渡過歡笑快樂的碩一。以及我的同學，邊衝浪邊做研究的正修，聰明搞笑的評翔，數值分析魔人政良，謝謝你們兩年來的陪伴！還有下一屆的學弟妹，認真的卓諭，厲害的麒宏，很有種的宣融，很愛模仿別人的紹展，講究的峻瑜，很麻吉的詩薇，努力的祖偉，因為有你們，實驗室總有歡笑的聲音，謝謝你們！

Content

List of Figures

List of Tables

Chapter 1

Introduction

Recent rapid progresses in wireless communication systems have created a need for dual-band operation for RF devices, such as the global systems for mobile communication systems (GSM) at 0.9/1.8 GHz and wireless local area network (WLAN) at 2.4/5.2 GHz. Bandpass filter are a vital device in the RF front ends of both receiver and transmitter. So high-performance microwave/RF bandpass filters are highly required in wireless communication systems. Recently, many planar dual-band bandpass filters have been proposed for synthesis methods [1]-[4], innovative design method [5]-[12], and circuit miniaturization [13]. In [1], a dual-band filter is realized by a bandstop filter and a wideband bandpass filter. In [2], the dual-passband response is designed by stepped-impedance resonators in both inline and parallel-coupled configurations. In [3], a systematic synthesis procedure is proposed to devise a dual-band bandpass filter. Series and parallel open stubs are used as resonators to fulfill the dual-band characteristics. On the basis of the same design concept in [3], a stepped-impedance coupled-line utilized as a dual-band inverter is introduced in [4].

Several structures have been developed for contriving novel dual-band bandpass filters. In [5], compact hairpin resonators are used to carry out two quasi-elliptic function passbands. The cross coupled filter in [6] has a very sharp transition since it possesses a transmission zero on the upper side of each passband. In [7], a resonator with a loaded open stub is adopted to implement a dual-band bandpass filter. In [8], two dual-mode resonators are utilized to obtain the dual-band response. Note that both two operation frequencies can be independently adjusted.

An ideal bandpass filter is expected to be free of spurious. The spurious responses are, however, one of the distributed natures. Recently, suppressing these unwanted responses has

become a popular issue [9]-[12]. In [9] and [10], the substrate suspension technique and dielectric overlay method are proposed for suppressing the second harmonic ($2f_o$). Based on providing different electric lengths for the even- and odd-modes, corrugated coupled-line microstrip is also an effective way for extending the upper stopband up to $3f_o$ [11]. In [12], multi-spurious suppression is fulfilled by choosing the constitutive resonators having identical passband frequency but staggered higher order resonances. It is noted that the structures in [9]-[12] are only involved with a single passband.

So far, it is still a challenge to design a dual-band bandpass filter with wide stopband. Only few relative papers have been published [13]-[14]. In [13], a rigorous design approach for a dual-band filter with broad upper stopband is disclosed. By means of designated coupling and resonator sections, spurious suppression could be readily achieved. In [14], various sizes of stepped-impedance resonators are established to contrive a filter with dual-passband and wide upper rejection. Each resonator is devised to possess two identical leading resonances but different higher order counterparts to make spurious peaks have low levels and small bandwidths. The results show a rejection level of 30 dB up to more than eight times of the fundamental frequency can be obtained.

In this thesis, an alternative design technique is proposed for building a bandpass filter with a dual-passband response with a broad upper stopband. The resonant frequencies of hairpin resonators are adjusted by three tapped open stubs to have two identical frequencies and dispersed higher-order resonances. Through the rejection enhanced by transmission zeros created due to various analytical techniques, a dual-band filter with exceptional performance can be carried out. In the following, Chapter 2 addresses the design idea and investigates the resonant property of a hairpin resonator with tapped open stubs and design procedure of band pass filter, also analyzes the transmission zeros of created by the coupled structure of the circuit, Chapter 3 demonstrates the simulation and measured results of two experimental circuits, and Chapter 4 draws the conclusion.

Chapter 2

Compact Hairpin Resonator Bandpass Filters with Dual-Band Response and Wide Stopband Procedure

In this chapter, a novel topology of a dual-band filter with broad upper stopband is proposed. Fig. 2.1-1 presents a third-order bandpass filter which constructed by hairpin resonator with tapped open stubs. The idea originates from dissimilar resonators in [12]. Since each resonator of this circuit has different sizes of open stubs, it could simultaneously have two identical operation frequencies and dispersed spurious harmonics. Based on the analogous procedure in [14], a dual-band filter with exceptional performance is finally carried out.

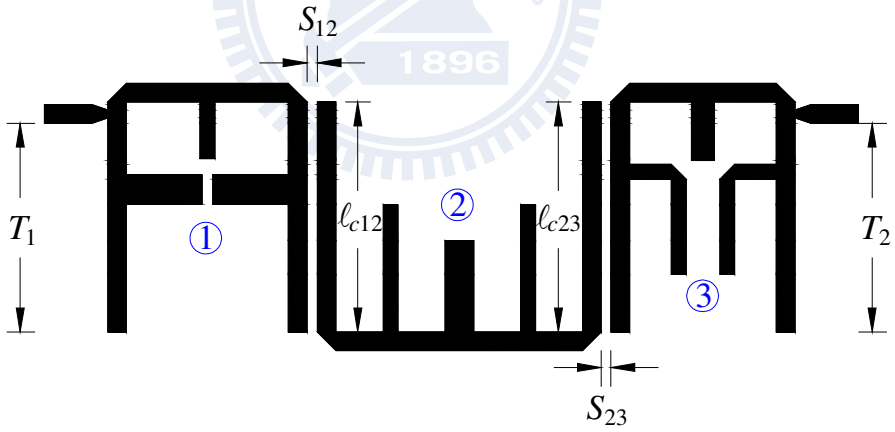

Fig. 2.1-1. Proposed third-order bandpass filter.

2.1 Hairpin Resonator with Taped Open Stubs

Fig. 2.1-2 shows the layout of the proposed hairpin resonator with tapped open stubs. It consists of one open stub (Z_1, θ_1) tapped at its center and two stubs (Z_2. θ_2) symmetrically located between its middle and edge. Since this structure is symmetric, we can use even- and odd-mode to analysis. With the aid of even- and odd-mode analysis [19], the resonance conditions can be easily formulated. For this miniaturized Hairpin resonator, the fundamental resonant frequency is odd mode resonance, and the first harmonic frequency is even mode resonance, therefore, analyzing the characteristic of these two modes is important for designing filter.

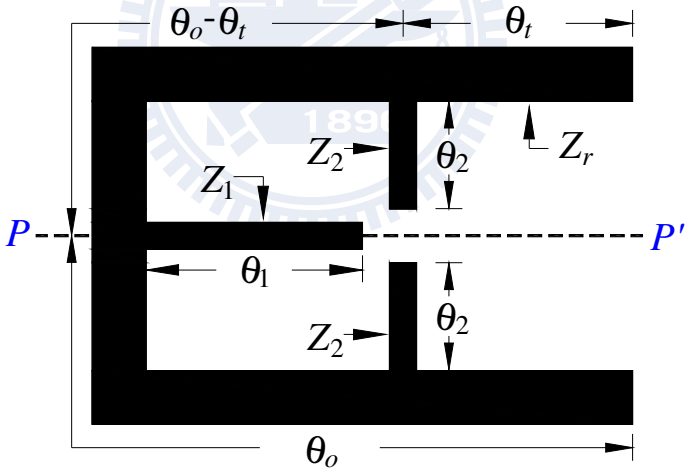

Fig. 2.1-2. Hairpin resonator with tapped open stubs.

The following, for simplicity to view, we use unfolded resonator Fig. 2.1-3 to formulate resonant mode conditions.

When the odd mode resonance occurs, the plane P-P' is equivalent to electric wall, means that the central of the resonator is virtual ground, as shown in Fig. 2.1-4. The resistance

looking into the resonator form P-P' plane to open end is zero. According to the microwave transmission theory [19], we would find:

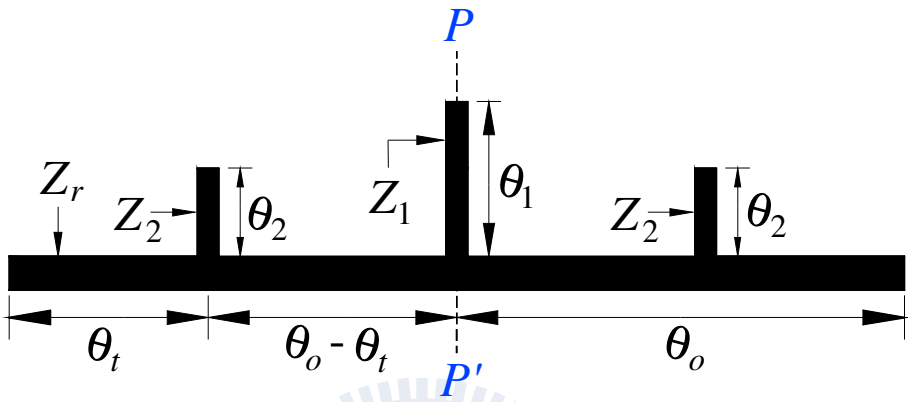

Fig. 2.1-3. Unfolded resonator with tapped open stubs.

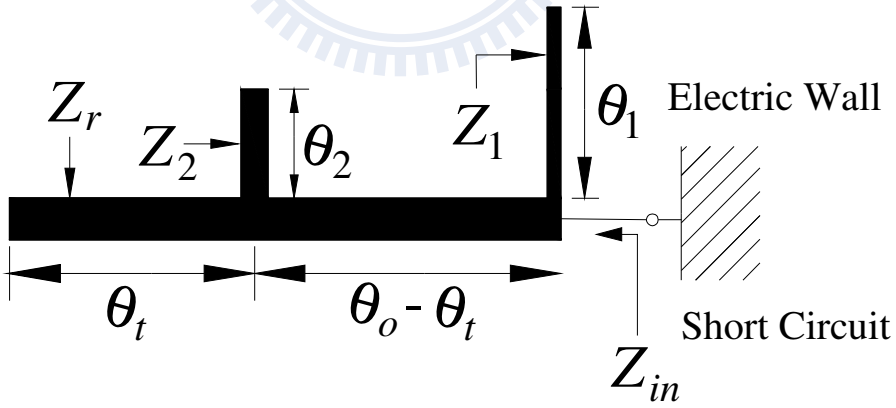

Fig. 2.1-4. Odd mode analysis of unfolded resonator.

$$Z_{in} = Z_r \frac{\dfrac{1}{j\dfrac{1}{Z_2}\tan\theta_2 + j\dfrac{1}{Z_r}\tan\theta_t} + jZ_r \tan(\theta_o - \theta_t)}{Z_r + \dfrac{\tan(\theta_o - \theta_t)}{\dfrac{1}{Z_2}\tan\theta_2 + \dfrac{1}{Z_r}\tan\theta_t}} = 0 \quad (2\text{-}1)$$

Simplify this equation, we get two conditions:

$$1 - \frac{Z_r}{Z_2}\tan\theta_2 \tan(\theta_o - \theta_t) - \tan\theta_t \tan(\theta_o - \theta_t) = 0 \quad (2\text{-}2a)$$

$$\frac{Z_r}{Z_2}\tan\theta_2 + \tan\theta_t + \tan(\theta_o - \theta_t) = \infty \quad (2\text{-}2b)$$

Only the 2-2a equation is reasonable to solve. We can rewrite 2-2a as follows; note that the odd mode resonance condition is independent of the center stub (Z_1, θ_1).

$$\frac{Z_r}{Z_2}\tan\theta_2 \tan(\theta_o - \theta_t) + \tan\theta_t \tan(\theta_o - \theta_t) - 1 = 0 \quad (2\text{-}3)$$

Similarly, when the even mode resonance occurs, the plane P-P' is equivalent to magnetic wall, means that the central of the resonator is open circuit, as shown in Fig. 2.1-5. The resistance looking into the resonator form P-P' plane to open end is infinite, so the admittance is zero. According to the microwave transmission theory [19], we would find:

$$Y_{in} = \frac{Z_r + \dfrac{j\tan(\theta_o - \theta_t)}{j\dfrac{1}{Z_2}\tan\theta_2 + j\dfrac{1}{Z_r}\tan\theta_t}}{Z_r\left(\dfrac{1}{j\dfrac{1}{Z_2}\tan\theta_2 + j\dfrac{1}{Z_r}\tan\theta_t} + jZ_r \tan(\theta_o - \theta_t)\right)} + j\frac{1}{2Z_1}\tan\theta_1 = 0 \quad (2\text{-}4)$$

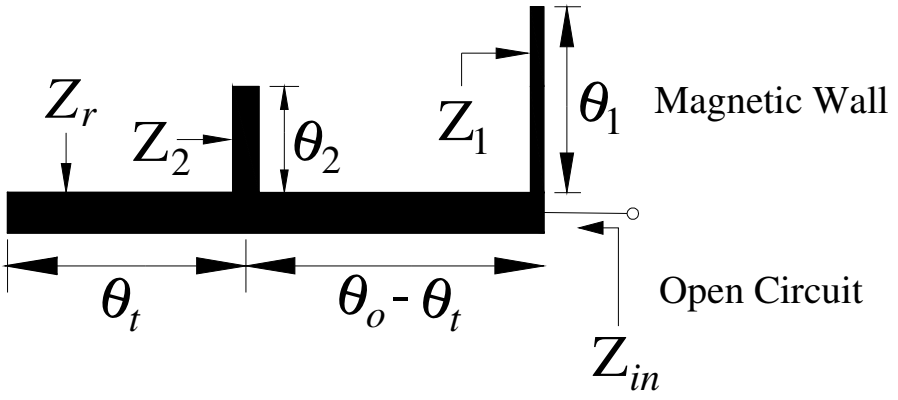

Fig. 2.1-5. Even mode analysis of unfolded resonator.

Simplified this equation, we get two conditions:

$$\frac{1}{Z_2}\tan\theta_2+\frac{1}{Z_r}\tan\theta_t+\frac{1}{Z_r}\tan(\theta_o-\theta_t)$$
$$+\frac{1}{2Z_1}\tan\theta_1\left[1-Z_r\tan(\theta_o-\theta_t)\left(\frac{1}{Z_2}\tan\theta_2+\frac{1}{Z_r}\tan\theta_t\right)\right]=0 \tag{2-5a}$$

$$1-Z_r\tan(\theta_o-\theta_t)\left(\frac{1}{Z_2}\tan\theta_2+\frac{1}{Z_r}\tan\theta_t\right)=\infty \tag{2-5b}$$

Only the 2-5a equation is reasonable to solve. We can rewrite 2-5a as follows:

$$\frac{Z_r}{Z_2}\tan\theta_2+\tan\theta_t+\tan(\theta_o-\theta_t)$$
$$+\frac{Z_r}{2Z_1}\tan\theta_1\left[\frac{1}{Z_r}-\tan(\theta_o-\theta_t)\left(\frac{Z_r}{Z_2}\tan\theta_2+\tan\theta_t\right)\right]=0 \tag{2-6}$$

In order to reduce the variables, we define impedance ratio as

$$R_1 = \frac{Z_r}{Z_1} \tag{2-7}$$

$$R_2 = \frac{Z_r}{Z_2} \tag{2-8}$$

Using the two resonance conditions, 2-3 and 2-6, we can draw the Fig. 2.1-6. Fig. 2.1-6 plots the resonant frequencies against θ_2 for the fundamental, first, second, and through to fifth higher order modes for $R_1 = 0.8$, $R_2 = 1.2$, $\theta_1 = 15°$, $\theta_t = 20°$, 40° and 60°. All electrical lengths are referred at f_1. The y-axis is the even- and odd-mode resonant frequencies of tapped open stubs resonator which is normalized with respect to the fundamental frequency f_0 of uniform impedance resonator. From Fig. 2.1-6, we found that when θ_2 =0, the odd mode resonances (independent of center stub Z_1, θ_1) equal to odd numbers. In Fig. 2.1-5, we can change the value of R_1, R_2, θ_1, θ_2, and θ_t to appropriately adjust the even- and odd-mode resonant frequencies.

Fig. 2.1-7 plots f_2 through f_6 normalized with respect to the fundamental frequency f_1 for various θ_2 and θ_t. Note that the data shown in Fig. 2.1-6 form an important basis of our design for determining the resonator geometry. Each resonator possesses the first two identical resonant frequencies f_1 and f_2, but has different higher order dispersed to make the spurious peaks can be made relatively low and then extend the upper stopband. In this thesis, the two operation frequencies f_1 and f_2 are respectively allocated as 2.4 GHz and 5.2 GHz. So, we should find a solution for a resonator to resonate at f_1 = 2.4GHz, and f_2 = 5.2GHz. Based on the conditions above, and have to make all resonators mutually disperse the high-order resonant frequency; it will restrict the solution to a small range. So as to loosen restrictions, it will be a selection to let f_3 = 5.2GHz, not f_2, nevertheless, f_1 is till 2.4GHz. In this third-order bandpass filter, the second resonator was chosen to resonate at f_1 = 2.4GHz, f_2 = 3.9GHz, and f_3 = 5.2GHz, that is different from the first and third resonator, it makes the high-order modes more spread out. The drawback is that $2\theta_o$ of second resonator will longer

than the other resonators 10% approximately.

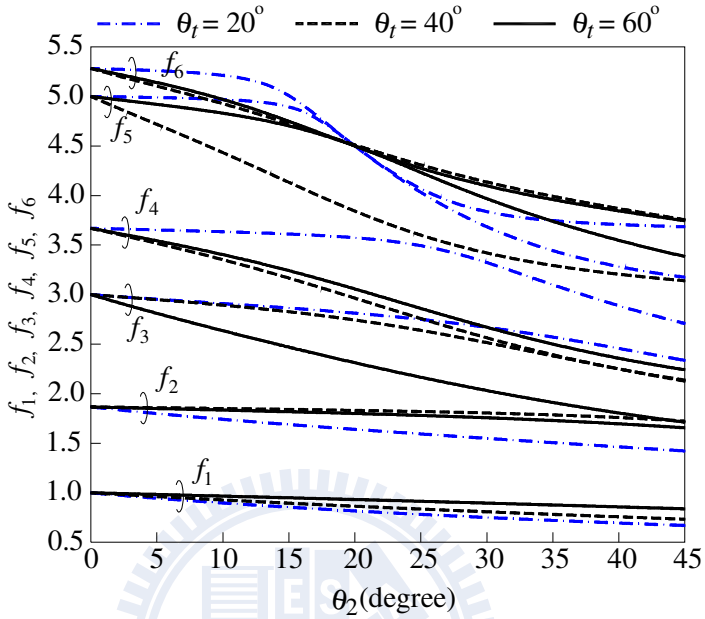

Fig. 2.1-6. Resonant spectrum with $\theta_t = 20°$, 40° and 60°. $R_1 = Z_r/Z_1 = 0.8$, $R_2 = Z_r/Z_2 = 1.2$, $\theta_1 = 15^o$.

Fig. 2.1-1 shows the layout of a third-order dual-band bandpass filter where Z_r of each resonator is chosen as 50 Ω, for the sake of avoiding high impedance of open stub that produces less radiation. Other dimensions of each resonator with respect to f_1 are listed in Table I. Fig. 2.1-8 shows the insertion loss |S21| frequency response from 0GHz to 20GHz of each resonators by gap excitation. Suppose the circuits are designed on a substrate with ε_r = 10.2 and thickness h = 0.635 mm. From this figure, we can see the resonance frequency positions of each resonator are mutually dispersed, except for the two operation frequencies f_1 and f_2.

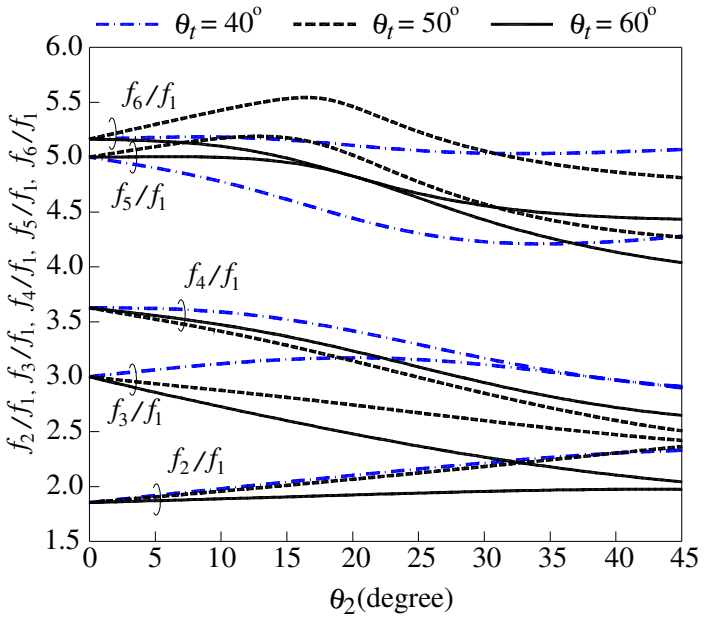

Fig. 2.1-7. Resonant spectrum with $\theta_t = 40^o$, 50^o and 60^o. $R_1 = Z_r/Z_1 = 0.8$, $R_2 = Z_r/Z_2 = 1.2$, $\theta_1 = 15^o$. All resonances are normalized with respect to the fundamental frequency f_1.

Table I.

Dimensions of each resonator in third-order dual-band bandpass filter.

	θ_t (^{o})	Z_1 (Ω)	θ_1 (^{o})	Z_2 (Ω)	θ_2 (^{o})
Res. 1	30.7	54.7	13.6	39.6	18.5
Res. 2	65.7	39.6	22.4	54.7	30.0
Res. 3	36.1	44.5	14.1	54.7	32.2

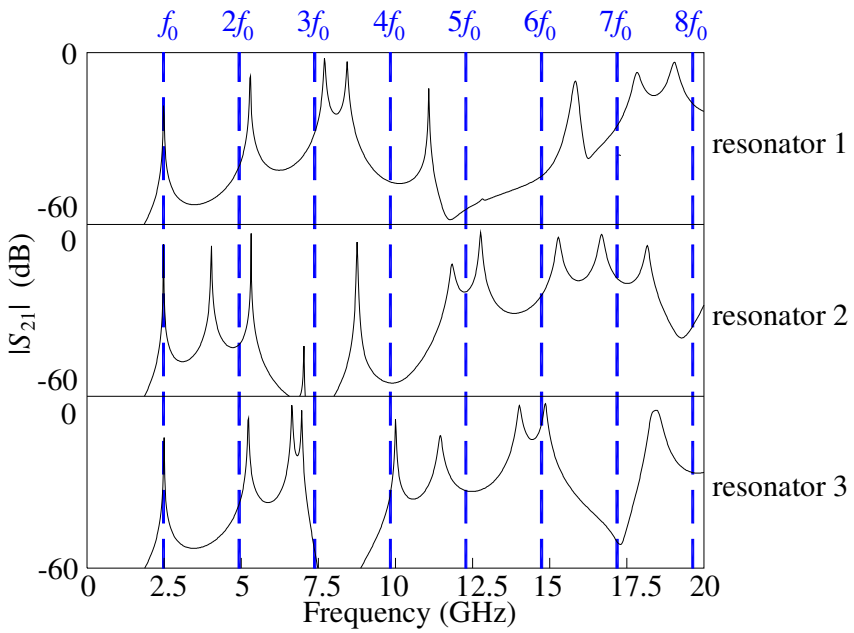

Fig. 2.1-8. Insertion loss |S21| of each resonator by third-order dual-band bandpass filter.

2.2 Coupling Length and Coupling Gap of Each Coupled Stage

Next, we determine the coupling scheme of each pair of adjacent resonators to meet the required coupling coefficients for two respective bands.

In synthesis of a bandpass filter with coupled resonators, the coupling coefficient between the *j*th and (*j* + 1)th resonators, $K_{j,j+1}$, is given by [15]:

$$K_{j,j+1} = \frac{\Delta}{\sqrt{g_j g_{j+1}}} \tag{2-9}$$

where g_j is element value of the low-pass filter prototype, and Δ is fractional bandwidth of bandpass filter. When two resonators have a close proximity, the coupling coefficient between two coupled resonators, K, is usually calculated by the approximation [16]:

$$K = \frac{f_a^2 - f_b^2}{f_a^2 + f_b^2} \tag{2-10}$$

In simulation by the IE3D, the two natural frequencies f_a and f_b of the two coupled resonators in Fig. 2.2-1 can be obtained by calculating the transmission response of the circuit with breaking the tap points and leaving a small gap to the input and output ports. Then use E-M simulator IE3D [20] to make electric-magnetic simulations of two adjacent resonators with various coupling length and coupling gap. Therefore, the relationship between coupling coefficient and coupling length or coupling gap is investigated.

Fig. 2.2-2 shows the coupling coefficient of two adjacent resonators with various coupling length or coupling gap for single frequency, h is the height of substrate, 0.635 mm.

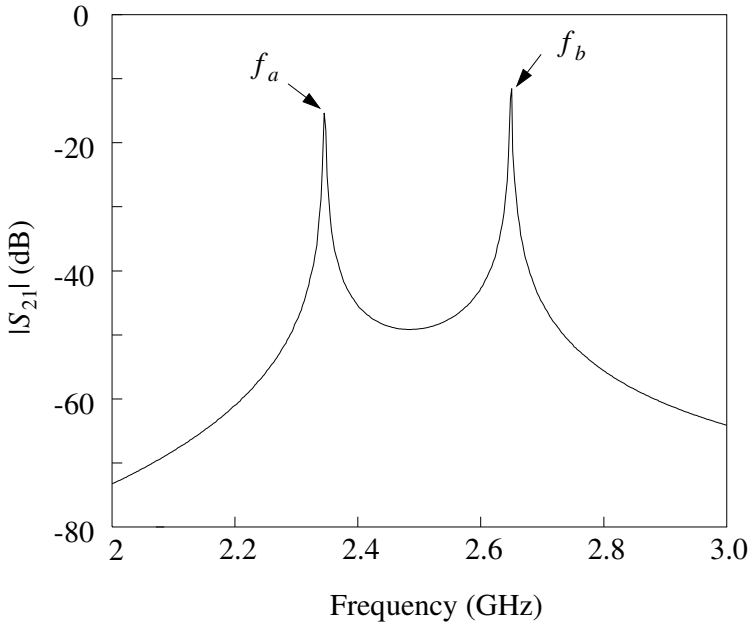

Fig. 2.2-1. Frequency Response of gap excitation of two adjacent resonators.

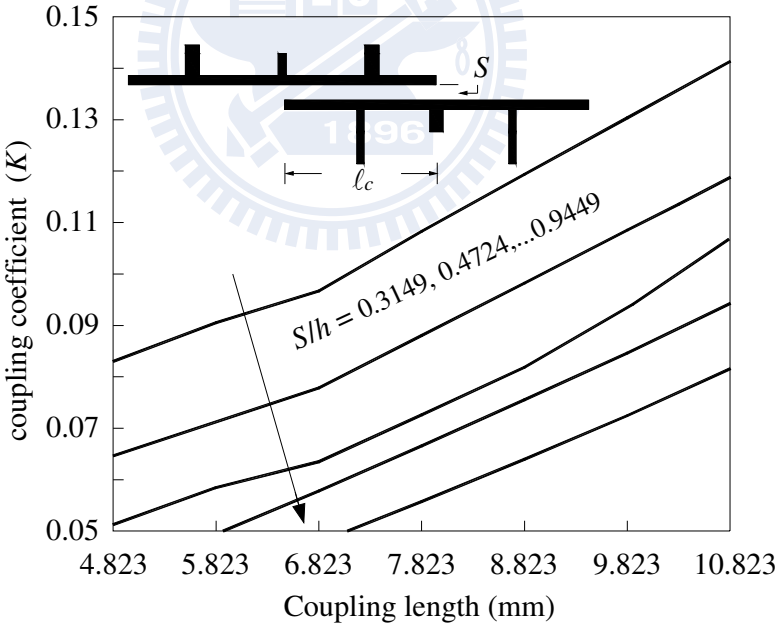

Fig. 2.2-2. Coupling coefficient with various coupling length or coupling gap for single frequency. Resonator 1: Z_r = 50 Ω, Z_1 = 52.2 Ω, θ_1 = 11.066°, Z_2 = 40 Ω, θ_2 = 15.7°, θ_t = 32.421°, Resonator 2: Z_r = 50 Ω, Z_1 = 41.667 Ω, θ_1 = 11.676°, Z_2 = 55.556 Ω, θ_2 = 25.591°, θ_t = 38.919°.

If a dual-band bandpass filter is desired, the two bands coupling coefficient need to be satisfied simultaneously:

$$\begin{cases} \left(K_{j,j+1}\right)_1 = \dfrac{\Delta_1}{\sqrt{(g_j g_{j+1})_1}} \\ \left(K_{j,j+1}\right)_2 = \dfrac{\Delta_2}{\sqrt{(g_j g_{j+1})_2}} \end{cases} \tag{2-11}$$

and the subscript 1 or 2 denotes the first or the second passband. Rewrite 2-11 as:

$$\begin{cases} \Delta_1 = (K_{j,j+1})_1 \times \sqrt{(g_j g_{j+1})_1} \\ \Delta_2 = (K_{j,j+1})_2 \times \sqrt{(g_j g_{j+1})_2} \end{cases} \tag{2-12}$$

According to the equations 2-10 and 2-12, we can build up a design graph of each bandwidth with various coupling length and coupling gap. The g_j value is Chenbyshev filter with a 0.1-dB ripple. As shown in Fig. 2.2.3, the x-axis and y-axis represent the bandwidth of first pass-band 2.4GHz and second pass-band 5.2GHz, respectively. Using the resonators in Table I. The coupling length and coupling gap of first coupled stage is indicated by ℓ_{c12} and S_{12}, to second coupled stage is indicated by ℓ_{c23} and S_{23}. In this figure, the area that two seashells overlapped is the fractional bandwidth capable to design dual-band bandpass filter. In order to maintain two passbands have sufficient bandwidth at the same time , we would select ℓ_{c12} = 7.25 mm and S_{12} = 0.325 mm, ℓ_{c23} = 7.25 mm and S_{23} = 0.3 mm, fractional bandwidth at 2.4GHz is 11.42%, and 5.35% at 5.2GHz.

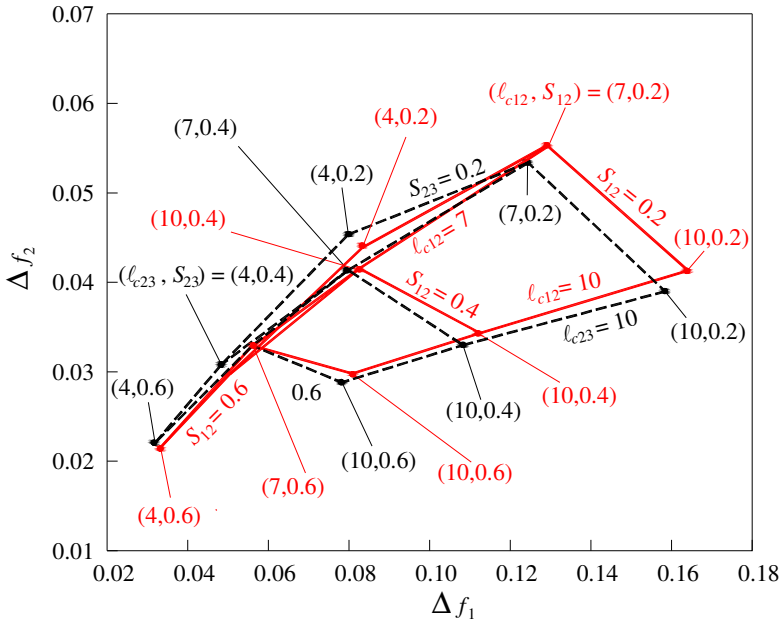

Fig. 2.2-3. Third-order bandpass filter fractional bandwidths of central frequency 2.4GHz, and 5.2GHz.

To appropriate input and output coupling for the bandpass filter, the tap positions which is specified by T_1, and T_2 in Fig. 2.1-1 should be determined by matching the singly loaded Q (Q_{si}) of the tapped resonator with the passband specification [17]. The singly loaded Q (Q_{si}) of the tapped resonator is defined as

$$Q_{si} = R_L \frac{\omega_0}{2} \frac{dB}{d\omega}\bigg|_{\omega_o} \tag{2-13}$$

where R_L is the impedance seen by the resonator looking toward the source/load, ω_0 is the operating frequency, and B is the input susceptance seen at the tap point looking into the resonator.

Besides, Q_{si} also can be described by the filter specification [18], written as

$$Q_{si} = \frac{g_o g_1}{FBW} \tag{2-14}$$

Combining equations 2-13 and 2-14, the relationship between R_L and tap position is derived as shown as follows:

$$R_L = \frac{2Q_{si}}{\omega_o \frac{\partial B(T_{in})}{\partial \omega}\Big|_{\omega_o}} = \frac{2\frac{g_o g_1}{FBW}}{\omega_o \frac{\partial B(T_{in})}{\partial \omega}\Big|_{\omega_o}} = \frac{2 g_o g_1}{\omega_o \cdot FBW \cdot \frac{\partial B(T_{in})}{\partial \omega}\Big|_{\omega_o}} \tag{2-15}$$

If two different frequencies are concerned, equation 2-15 should be directed against 2.4GHz and 5.2GHz:

$$\begin{cases} R_{L1} = \dfrac{2 g_o g_1}{\omega_1 \cdot FBW_1 \cdot \dfrac{\partial B_1(T_{in})}{\partial \omega}\Big|_{\omega_1}} \\ R_{L2} = \dfrac{2 g_o g_1}{\omega_2 \cdot FBW_2 \cdot \dfrac{\partial B_2(T_{in})}{\partial \omega}\Big|_{\omega_2}} \end{cases} \tag{2-16}$$

We substitute the fractional bandwidth that described above into equation 2-16, and calculate the differential of susceptance from tap in, and tap out resonators, Fig. 2.2-4 plots the R_L versus tap position for input, and output resonators, T_{in} is the length from tap position to open end, as shown as Fig. 2.2-5. Since we want to miniaturize the bandpass filter, so it does not like to add an impedance transformer additionally, that increase the overall area of this filter. Instead of, we prefer to tap the position on the resonator that R_L is 50 Ω for f_1 and f_2 both. In Fig. 2.2-4, we can find that when tap at T_1 = 6.457 mm for input resonator, and at T_2 = 6.448 mm for output resonator, R_L is close to 50 Ω for both f_1 and f_2. Finally, the transmission zeros arise from tapping is shown as Fig. 2.2-6, Fig. 2.2-6 depicts the frequency response

simulated by making the other port gap excitation, as Fig. 2.2-7.

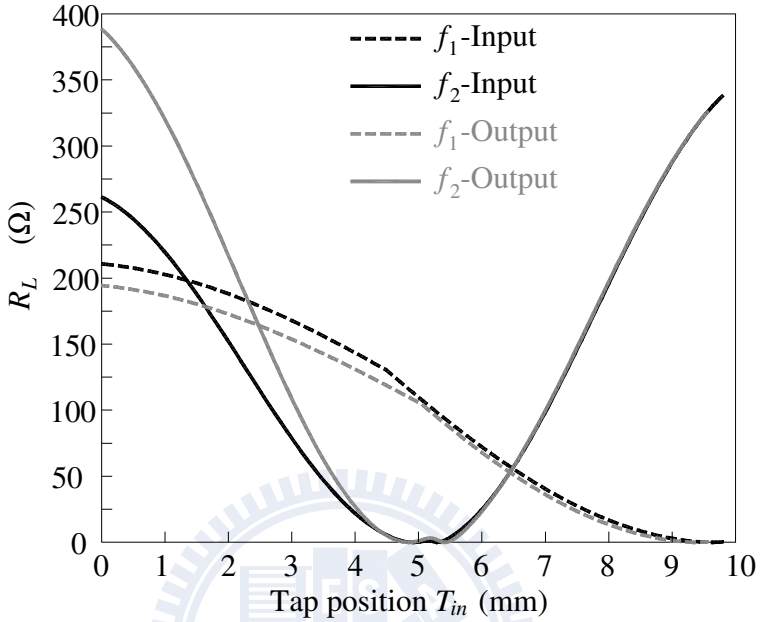

Fig. 2.2-4. Fractional bandwidths of central frequency 2.4GHz, and 5.2GHz for third-order filter.

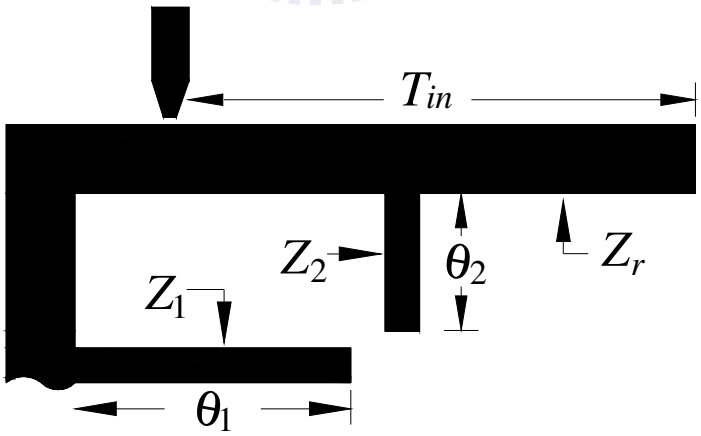

Fig. 2.2-5. Tap point on the resonator.

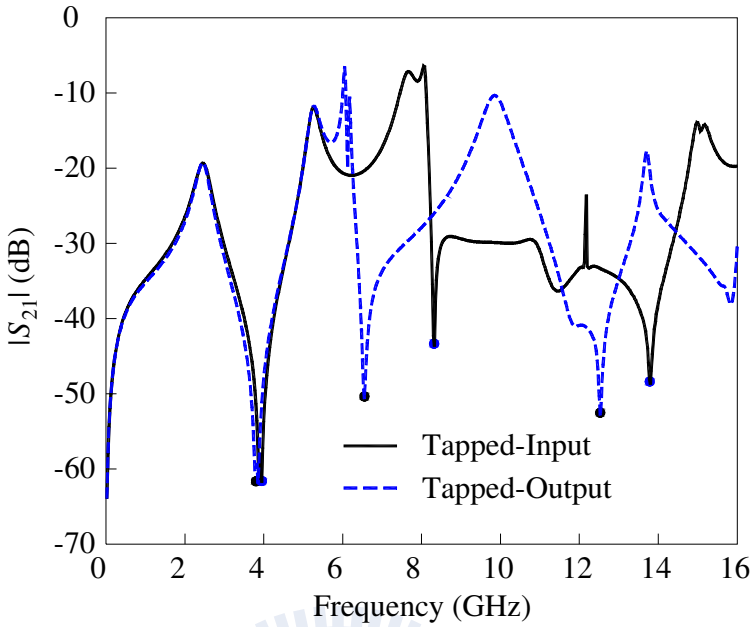

Fig. 2.2-6. Third-order bandpass filter Transmission zeros arise from tapping.

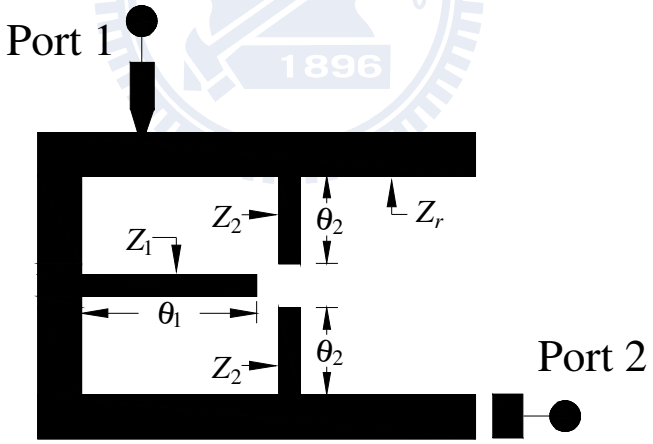

Fig. 2.2-7. Simulate tapping zeros by making the other port gap excitation.

The transmission zeros arise from tapping also can be calculated by numerical analysis, as shown as Fig. 2.2-8, the input impedance seen form tapped in point to open end is:

$$Z_{in} = Z_r \frac{\frac{1}{Z_r} + j\left(-j\frac{1}{Z_r}\tan\theta_t - j\frac{1}{Z_2}\tan\theta_2\right)\tan(\theta_{Tin} - \theta_t)}{-j\frac{1}{Z_r}\tan\theta_t - j\frac{1}{Z_2}\tan\theta_2 + j\frac{1}{Z_r}\tan(\theta_{Tin} - \theta_t)} \tag{2-15}$$

When Z_{in} equal to zero, the transmission zeros arise from tapping is occurred. Fig. 2.2-9 depicts the spectrum of tapped zeros included tapped in and tapped out resonators.

If we change the tap position, may alter the transmission zeros to desired frequencies [14], but, for same reason, it will need an extra impedance transformer to match the R_L for both f_1 and f_2.

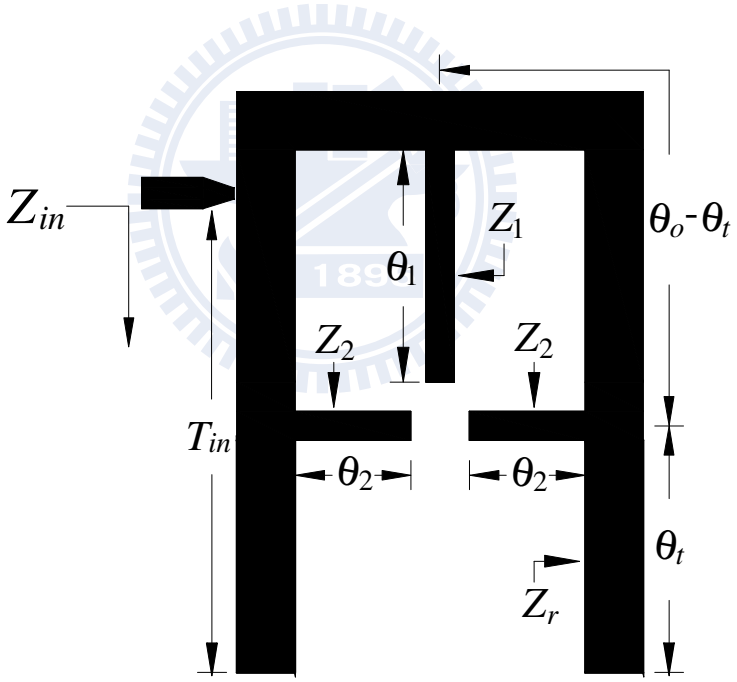

Fig. 2.2-8. Calculate transmission zeros arise from tapping by making Z_{in} equal to zero.

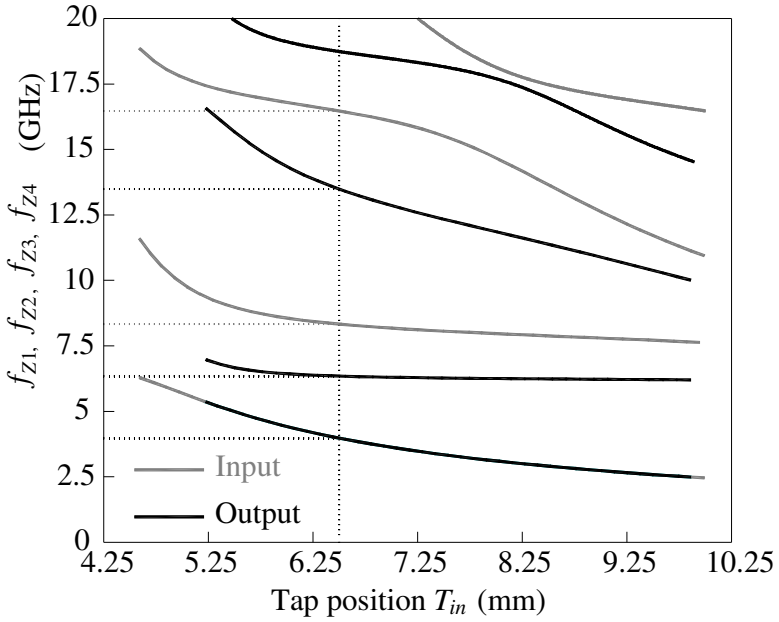

Fig. 2.2-9. Spectrum of tapping zeros included tapped in and tapped out resonators.

2.3 Transmission Zeros of Coupled Stage

Since our target is to design a dual-band filter with a wide stopband, the zeros are created by each coupled stage are required to investigate carefully. Fig. 2.3-1. depicts the hairpin coupled-line section with tapped open stubs and its responses of simulation are plotted in Fig. 2.3-2. Note that the horizontal axis is normalized to the first operation frequency f_1. Suppose the circuits are designed on a substrate with ε_r = 10.2 and thickness h = 0.635 mm. Such a high dielectric substrate is purposely chosen to demonstrate performance of our approach. The simulation data are obtained by the full-wave software simulator IE3D [20]. Fig. 2.3-2(a) draws the $|S_{21}|$ of a coupled section with various θ_t. The circuit parameters are listed in the figure caption. Note that three transmission zeros will be observed from $3f_1$ to $6f_1$ and all zeros can be arbitrarily tuned by altering θ_t. Fig. 2.3-2(b) demonstrates the insertion results of a coupled-line stage with various θ_2. As θ_2 is increased, we expect that zeros would shift to a lower frequency. It can be deduced that a wide stopband could be readily achieved by adequately selecting each coupled section to suppress dispersed spurious peaks of a bandpass filter.

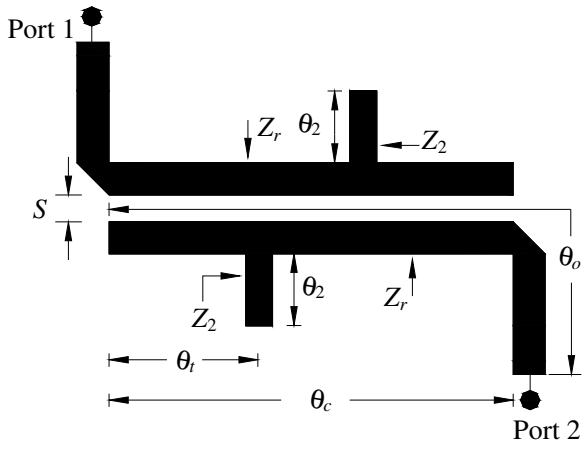

Fig. 2.3-1. Hairpin coupled-line section.

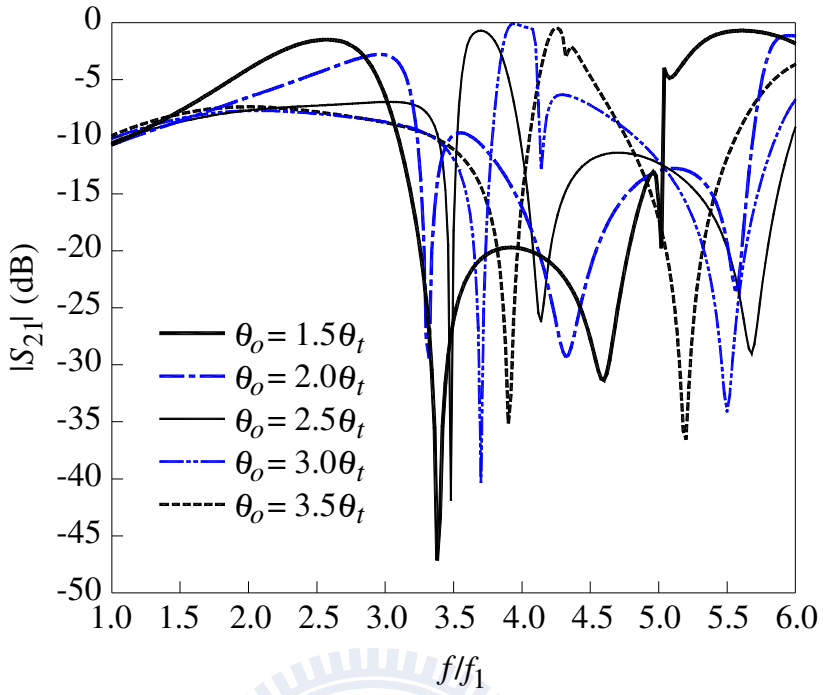

Fig. 2.3-2(a). Simulation responses of Fig. 2.3-1. with various θ_t where $\theta_2 = 17.5^{\circ}$. Other circuit size: $Z_r = 50\ \Omega$, $Z_2 = 52.2\ \Omega$, $\theta_o = 56.1^{\circ}$, and $S/h = 0.3937$.

Therefore, if there still have some spurious modes in the frequency response, not be suppressed yet, given different θ_2 and θ_t to control the transmission zero arise from the coupled stage to eliminate that. For desired transmission zero, Fig. 2.3-3 plots the frequency spectrum against θ_1 of three different resonators with various θ_2, and θ_t. Nevertheless, alter the value of θ_2 and θ_t make changes in the distribution of high-order modes, it would turn out that not to be dispersed with the other resonators'. So the trade off between disperse spurious and control transmission zero should be concerned to optimize the rejection band.

Fig. 2.3-4 plots the coupled stage frequency response of third-order bandpass filter Fig. 2.1-1, this figure shows the transmission zero arise from coupled stage 1, and coupled stage 2. From the stage 1, transmission zeros 6.96GHz, 8.77GHz, and 12.75GHz are introduced, and transmission zeros 6.45GHz, 6.9GHz, and 10.44GHz are caused from the stage 2.

The success of the wide upper stopband relies quite much on Fig. 2.3-5 which is an useful design graph, showing the zeros created by individual coupled-line sections and resonant peaks of the resonators. In the upper part of the plot, the rectangular boxes in the gray area represent the rejection bands produced by coupled-line sections. The widths of the boxes are defined as $|S_{21}|$ smaller than -15 dB. The coupling C_{01} and C_{34} match the external Q values of the end resonators with the two bandwidths by tapping. The tapped input and output can also be designed to create transmission zeros [14]. The lower part of Fig. 2.3-5 shows the resonant frequencies of the resonators. All of them are designed to have resonant frequencies at 2.4 and 5.2 GHz, and also have dispersed resonances, now the purpose of Fig. 2.3-5 becomes clear. To extend the stopband, the stopbaands created by the coupled sections have to cover the spurious peaks.

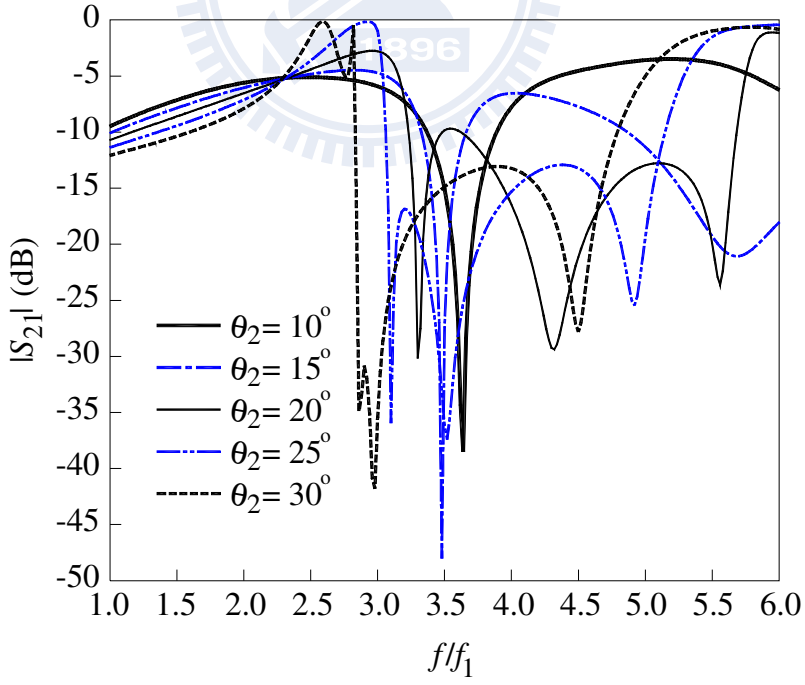

Fig. 2.3-2(b). Simulation responses of Fig. 2.3-1. with various θ_2 where θ_t = 34.6°. Other circuit size: Z_r = 50 Ω, Z_2 = 52.2 Ω, θ_o = 56.1°, and S/h = 0.3937.

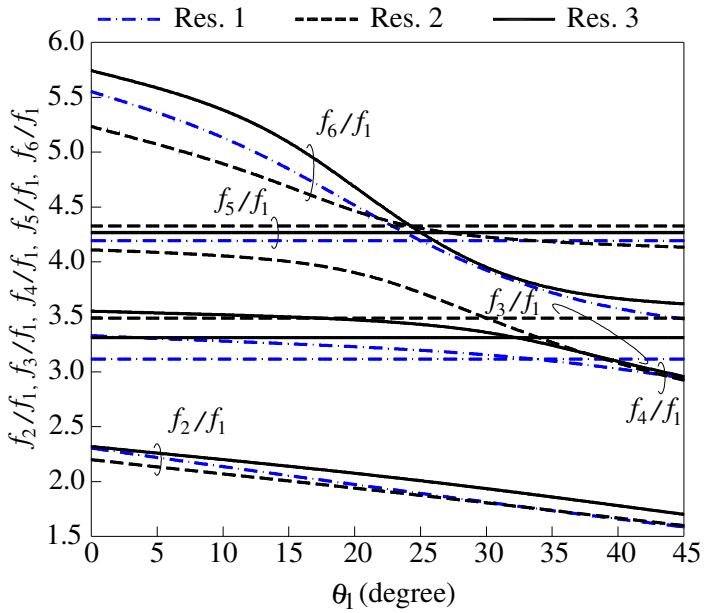

Fig. 2.3-3. Resonant spectrum against θ_1. All resonances are normalized with respect to the fundamental frequency f_1. The physical parameters in Fig. 2.3-3 are as follows; Res. 1: R_1 = 1.2, R_2 = 1, θ_2 = 25°, θ_t = 40°.Res. 2: R_1 = 1, R_2 = 1, θ_2 = 20°, θ_t = 30°. Res. 3: R_1 = 0.8, R_2 = 1.2, θ_2 = 22.2°, θ_t = 37.5°.

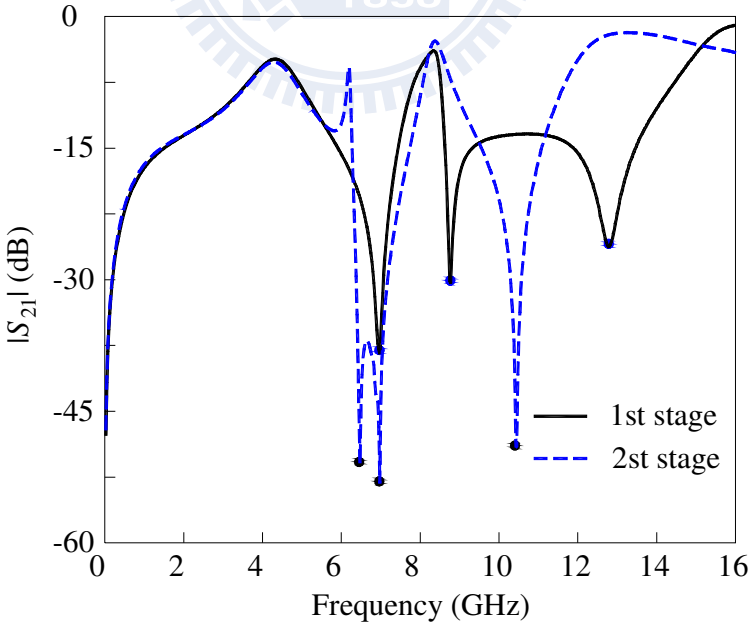

Fig. 2.3-4. Coupled stage frequency response of third-order bandpass filter.

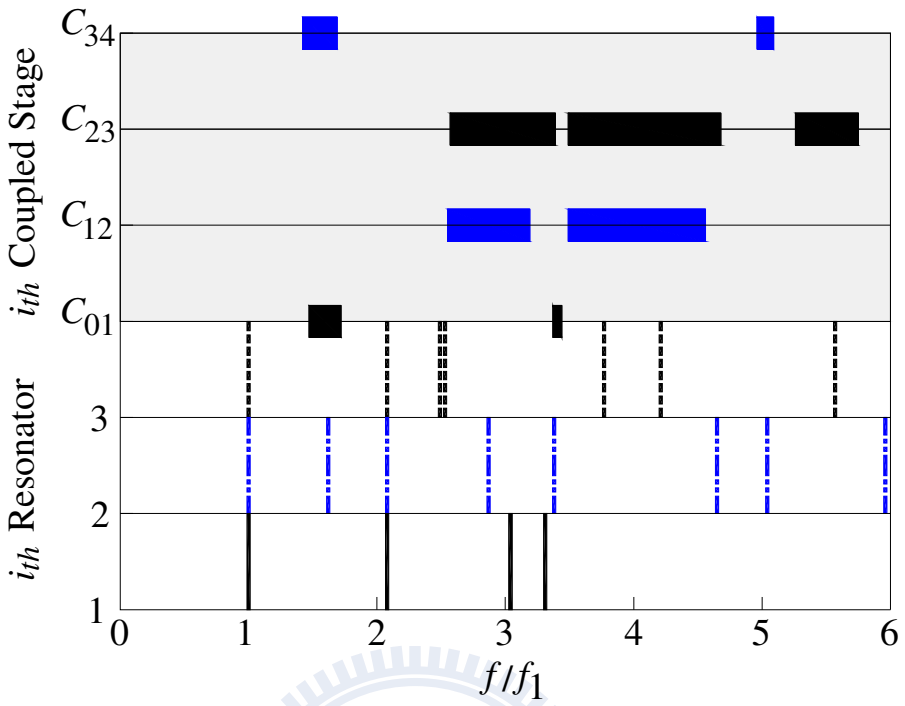

Fig. 2.3-5. Design graph for third-order resonators with resonances and transmission zeros.

2.4 Fifth-Order Dual-Band Bandpass Filter with Wide Stopband

This section we will summarize the filter design procedure, and introduce the second circuit, fifth-order dual-band bandpass filter.

At beginning, solve the two resonance conditions, 2-3 and 2-6, to figure out the resonator that resonates at two identical operation frequencies, and also disperses the high-order modes mutually. Fig. 2.4-1 shows the layout of a fifth-order dual-band bandpass filter where Z_r of each resonator is chosen as 50 Ω, prevent the radiation from high impedance of open stub. Dimensions of the five stub-tapped hairpin resonators are listed in Table II, where the electric lengths are evaluated at f_1. Two operational frequencies are chosen as 2.4GHz, and 5.2GHz. Fig. 2.4-2 shows the insertion loss |S21| of each resonator by fifth-order dual-band bandpass filter.

Second, according to equations 2-10 and 2-12, draw the figure of two bands' fractional bandwidth with various coupling length and coupling gap, the g value is Chenbyshev filter with a 0.1-dB ripple, Fig 2.4-3 depicts the four coupled stage, ℓ_{cij} and S_{ij} present the coupling length and coupling gap between *i*th and *j*th resonators. The area of four seashells overlapped is a quite small range in the center of this figure. We choose S_{12} = 0.275 mm, S_{23} = 0.46 mm, S_{34} = 0.44 mm, S_{45} = 0.265 mm, $\ell_{c12} = \ell_{c45}$ = 7.25 mm, and $\ell_{c23} = \ell_{c34}$ = 7.075 mm for Δf_1 = 12.12%, and Δf_2 = 6.84%. Then use equation 2-16 determine the tap position T_{in} for input and output resonators, Fig. 2.4-4 plots the R_L against the tap position with two concerned frequencies, we can figure out that intersection point of f_1 and f_2 is on $T_1 = T_2$ = 6.75 mm by R_L = 63 Ω for input and output resonators both, not 50 Ω. In order to obtain a better response without adding an extra impedance transformer, we adjust the tap position to $T_1 = T_2$ = 7.2 mm. Fig. 2.4-5 shows the frequency response calculated by gap excitation for tap in zeros.

Finally, investigate the coupled section zeros, tuning θ_2 and θ_t to control the coupled-line zeros to suppress unexpected peaks. Fig 2.4-6 plots the coupled stage frequency response of fifth-order bandpass filter Fig. 2.4-1, this figure shows the transmission zero arise from coupled stage 1 to coupled stage 4.

Fig. 2.4-7 summarizes the overall transmission zeros on the upper part, the lower part of Fig. 2.4-7 shows the resonant frequencies of the resonators. All of them are designed to have resonant frequencies at 2.4 and 5.2 GHz, but have dispersed resonances.

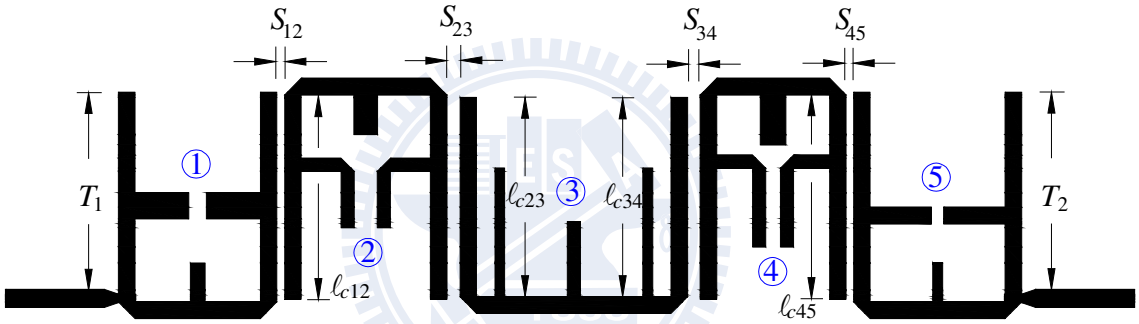

Fig. 2.4-1. Proposed fifth-order bandpass filter.

Table II.

Dimensions of each resonator in fifth-order dual-band bandpass filter.

	θ_t (°)	Z_1 (Ω)	θ_1 (°)	Z_2 (Ω)	θ_2 (°)
Res. 1	27.4	51.9	10.4	39.6	14.8
Res. 2	35.1	41.4	10.9	54.7	25.7
Res. 3	57.3	54.7	20.0	61.6	33.9
Res. 4	34.1	54.7	20.0	54.7	25.7
Res. 5	31.0	61.4	10.4	49.4	16.7

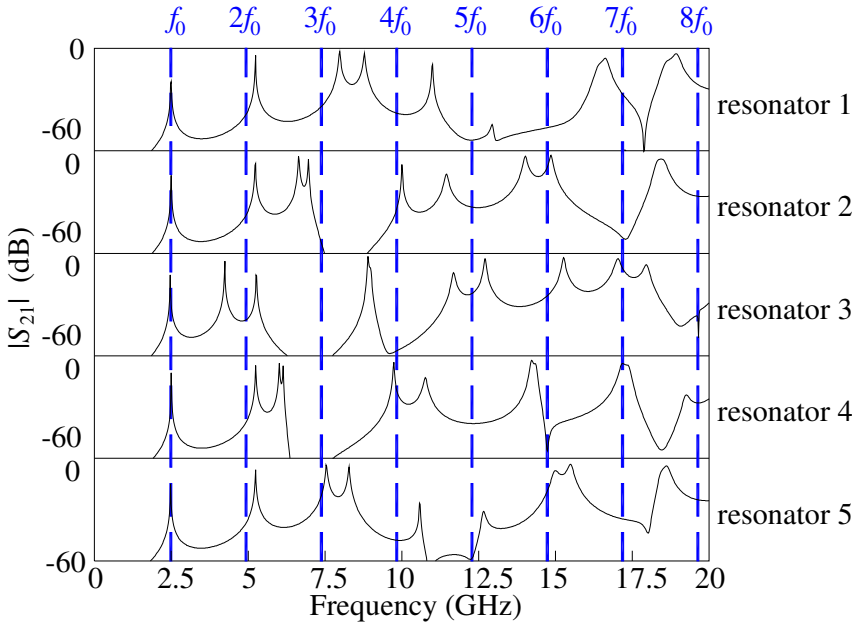

Fig. 2.4-2. Insertion loss |S21| of each resonator by fifth-order dual-band bandpass filter.

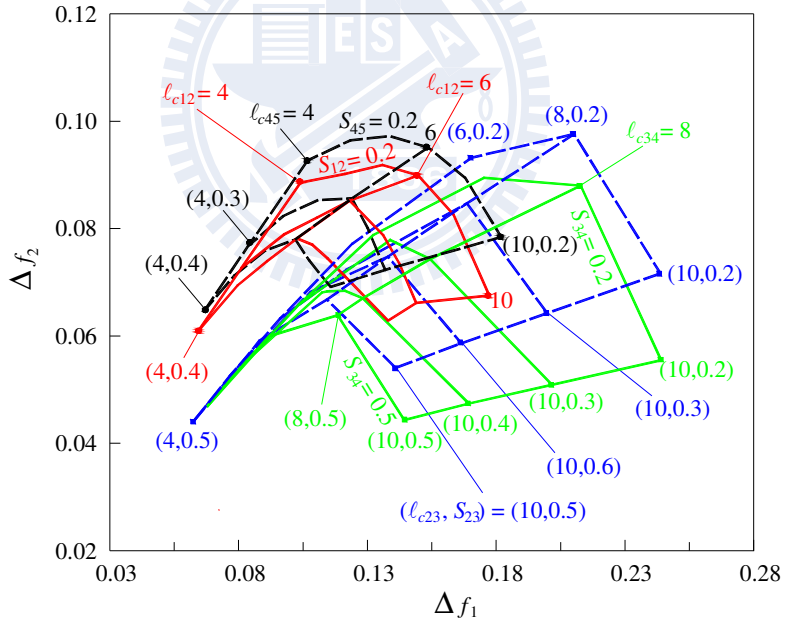

Fig. 2.4-3. Third-order bandpass filter fractional bandwidths of central frequency 2.4GHz, and 5.2GHz.

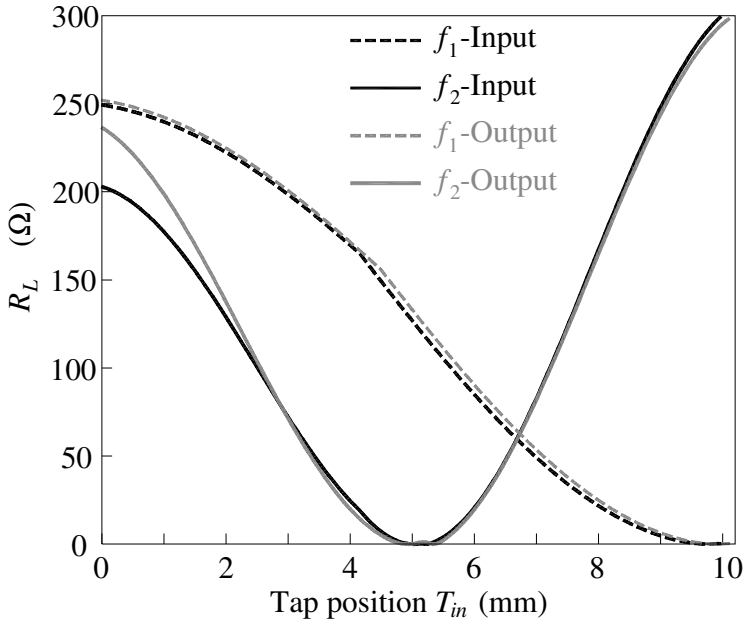

Fig. 2.4-4. Fractional bandwidths of central frequency 2.4GHz, and 5.2GHz for fifth-order filter.

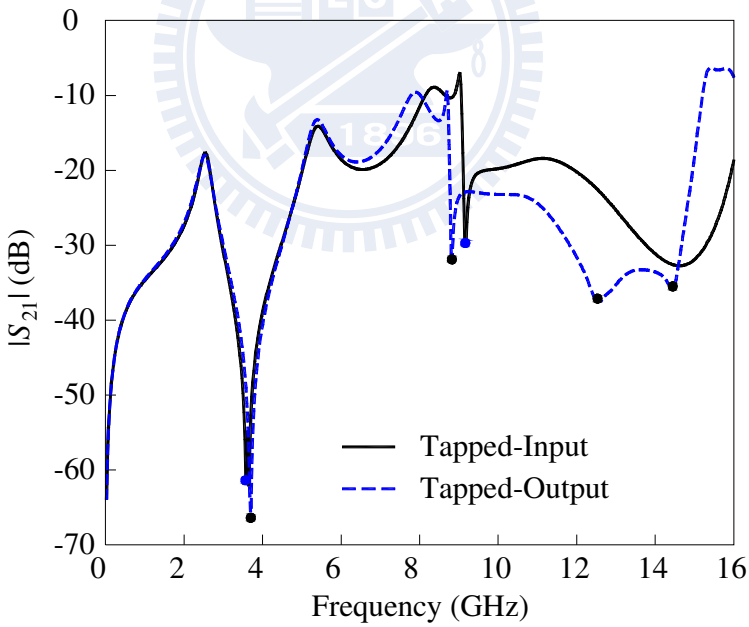

Fig. 2.4-5. Fifth-order bandpass filter transmission zeros arise from tap in.

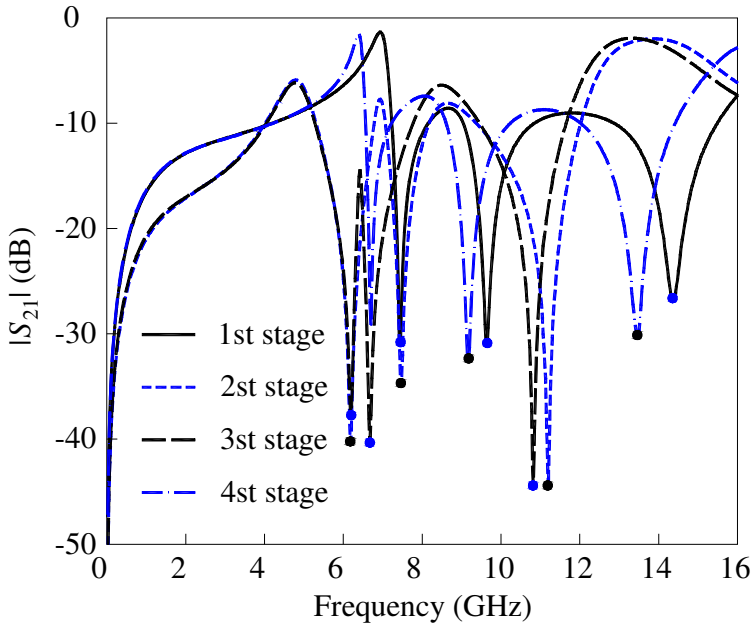

Fig. 2.4-6. Coupled stage frequency response of fifth-order bandpass filter.

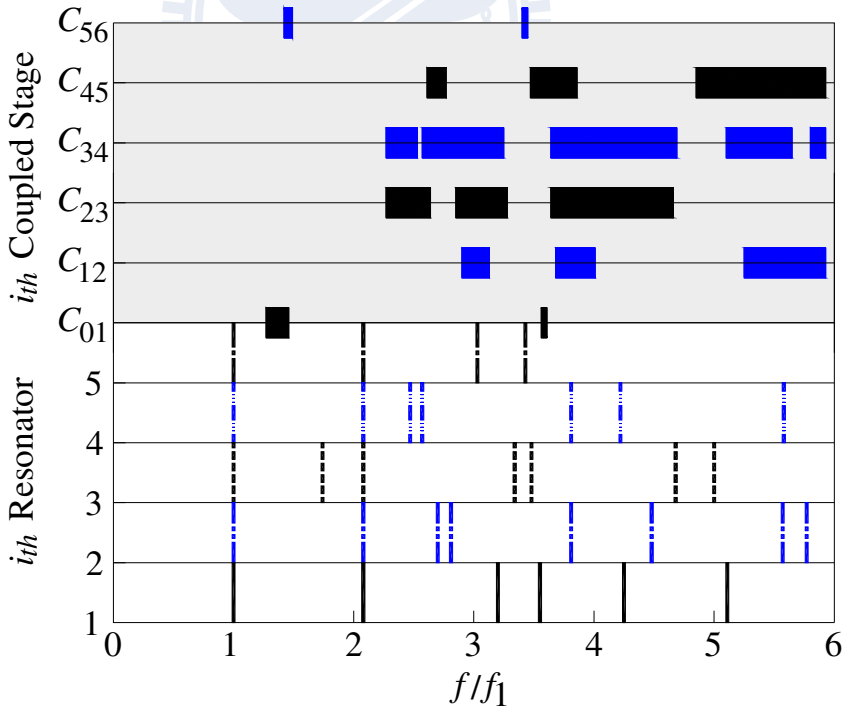

Fig. 2.4-7. Design graph for fifth-order resonators with resonances and transmission zeros.

Chapter 3

Simulation and Measurement

Two circuits are realized to validate our design idea. Fig. 3-1(a) plots the simulation and measured responses of the third-order experimental circuit. In both passbands, $|S_{11}|$ and $|S_{21}|$ are approximately -18 dB and -2.2 dB, respectively. The isolation between two passbands is approximately -40 dB. The -3 dB bandwidths are 12.19 % and 6.07% at the two designated bands. A stopband which is better than -23 dB up to $6f_1$ can be observed.

Fig. 3-1(b) demonstrates the performance of a trial fifth-order bandpass filter. The design procedure is similar to that of the previous. Fig. 3-1(b) compares the simulation and measured responses. The insertion loss and return loss in both passbands are about -3 dB and -17 dB, respectively. The -3 dB bandwidths at f_1 and f_2 are 9.86 % and 5.26 %, respectively. Since more coupled-line sections can be used to eliminate more spurious peaks, the rejection performance of this filter in the stopband is better than that of the third-order circuit. The measured results show that a rejection level better than -28 dB can be reached up to $6f_1$. Reasonably good agreement between simulation and measured results can be observed. In spite of obtaining a better rejection band, as trade off, higher order circuits usually accompany an increase of circuit area and more loss due to metal. Fig. 3-2 is the photograph of the measured filter.

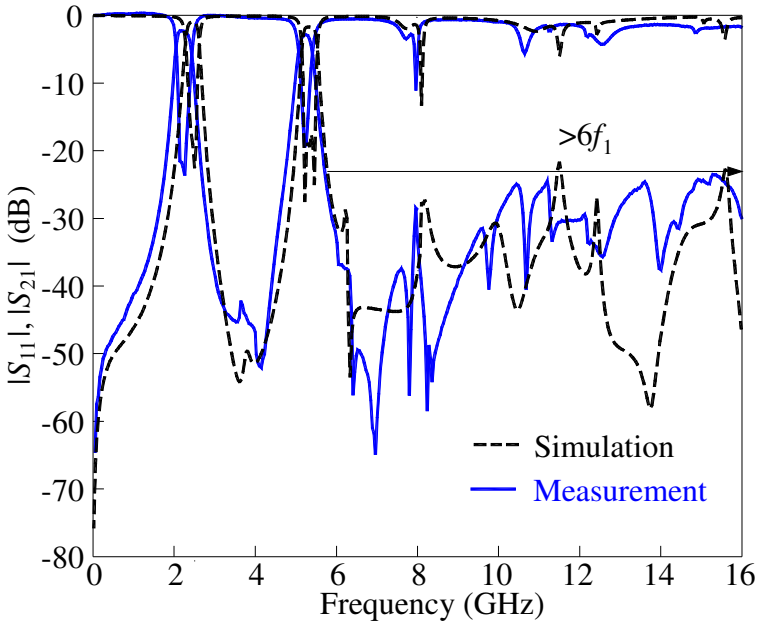

(a)

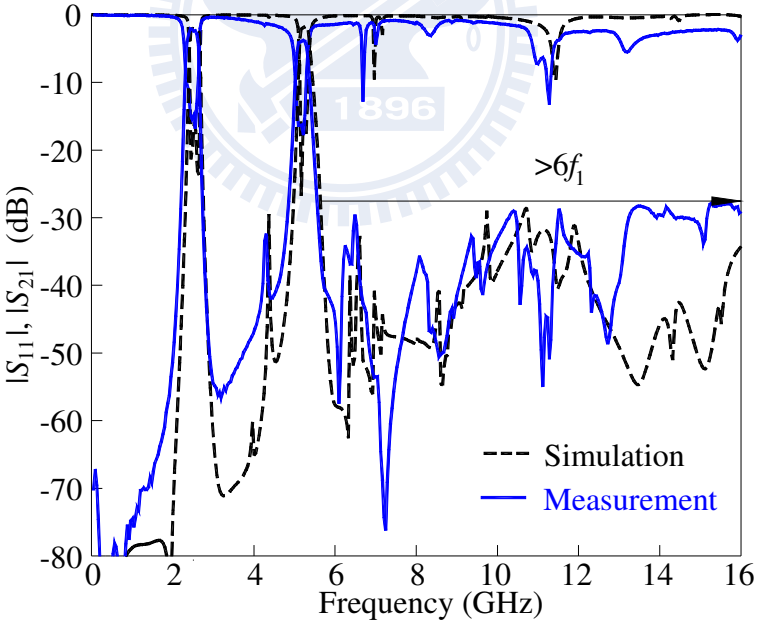

(b)

Fig. 3-1. Simulation and measurement results. (a) Third-order, (b) Fifth-order dual-band bandpass filter.

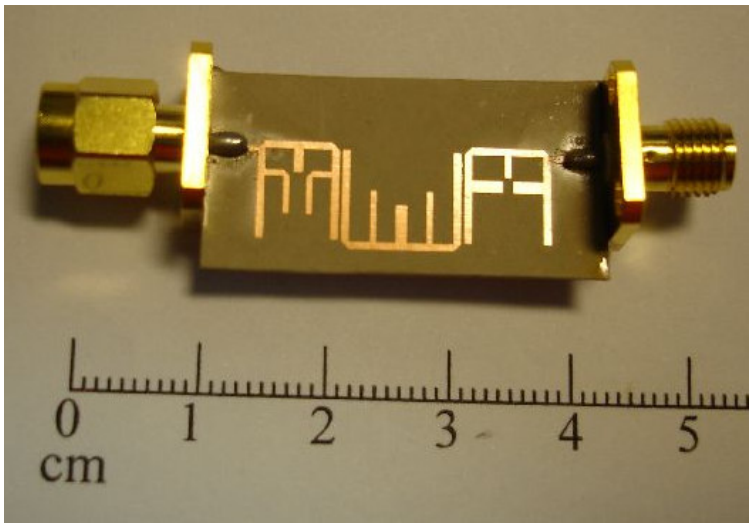

(a)

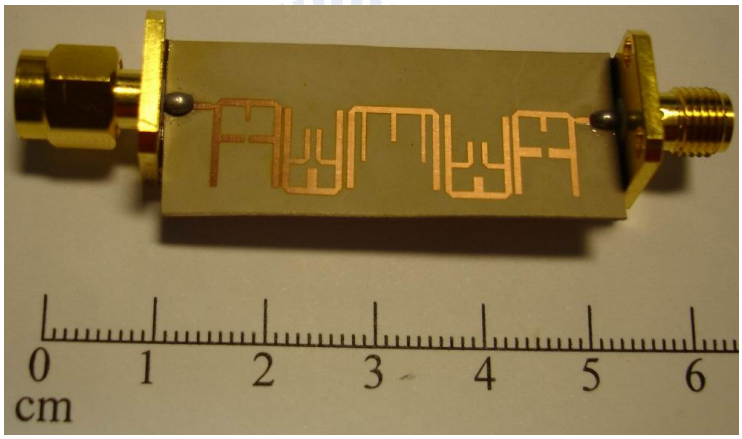

(b)

Fig. 3-2. Circuit photograph of the (a) Third-order, and (b) Fifth-order dual-band bandpass filter.

Chapter 4

Conclusion

Dual-band bandpass filter is equipped with a wide upper stopband by using hairpin resonators with tapped open subs. Those open stubs have different geometric parameters so that all modified resonators have two identical designated resonant frequencies and different higher-order resonances. To enhance the filter performance in the stopband, the transmission zeros created by the coupling structures are carefully configured to achieve multi-spurious suppression. Design graph of resonant peaks and stopband is plotted to facilitate the wide stopband design. Measurement indicates that rejection of better than -28 dB can be obtained for extension up to over six times the first resonance frequency. The measured results have good agreement with the simulation.

References

[1] L.-C. Tsai and C. W. Hsue, "Dual-band bandpass filters using equal-length coupled-serial-shunted lines and *Z*-transform technique," *IEEE Trans. Microwave Theory Tech.*, vol. 52, no. 4, pp. 1111-1117, Apr. 2004.

[2] J.-T. Kuo, T.-H. Yeh and C.-C. Yeh, "Design of microstrip bandpass filters with a dual-passband response," *IEEE Trans. Microwave Theory Tech.*, vol. 53, no. 11, pp. 1331-1337, Nov. 2005.

[3] C.-M. Tsai, H.-M. Lee and C.-C. Tsai, "Planar filter design with fully controllable second passband," *IEEE Trans. Microwave Theory Tech.*, vol. 53, no. 11, pp. 3429-3439, Nov. 2005.

[4] H.-M. Lee and C.-M. Tsai, "Dual-band filter design with flexible passband and bandwidth selections," *IEEE Trans. Microwave Theory Tech.*, vol. 55, no. 5, pp. 1002-1009, May. 2007.

[5] J.-T. Kuo and H.-S. Cheng, "Design of quasi-elliptic function filters with a dual-passband response," *IEEE Microwave Wireless Compon. Lett.*, vol. 14, no. 10, pp. 472-474, Oct. 2004.

[6] C.-C. Chen, "Dual-band bandpass filter using coupled resonator pairs," *IEEE Microwave Wireless Compon. Lett.*, vol. 15, no. 4, pp. 259-261, Apr. 2005.

[7] P. Mondal and M. K. Mandal, "Design of dual-band bandpass filters using stub-loaded open-loop resonators," *IEEE Trans. Microwave Theory Tech.*, vol. 56, no. 1, pp. 150-155, Jan. 2008.

[8] X. Y. Zhang and Q. Xue, "Novel dual-mode dual-band filters coplanar-waveguide-fed ring resonators," *IEEE Trans. Microwave Theory Tech.*, vol. 55, no. 10, pp. 2183-2190, Oct. 2007.

[9] J.-T. Kuo, M. Jiang, and H.-J. Chang, "Design of parallel-coupled microstrip filters with suppression of spurious resonances using substrate suspension," *IEEE Trans. Microwave Theory Tech.*, vol. 52, no. 1, pp. 83-89, Jan. 2004.

[10] J.-T. Kuo and M. Jiang, "Enhanced microstrip filter design with a uniform dielectric overlay for suppressing the second harmonic response," *IEEE Microwave Wireless Comp. Lett.*, vol. 14, no. 9, pp. 419-421, Sept. 2004.

[11] J.-T. Kuo, W.-H Hsu, and W.-T. Huang "Parallel coupled microstrip filters with suppression of harmonic response," *IEEE Microwave Wireless Comp. Lett.*, vol. 12, no. 10, pp. 383-385, Oct. 2002.

[12] C.-F. Chen, T.-Y. Huang and R.-B. Wu, "Design of microstrip bandpass filters with multi-order spurious-mode suppression," *IEEE Trans. Microwave Theory Tech.*, vol. 53, no. 12, pp. 3788-3793, Dec. 2005.

[13] K.-K. M. Cheng and C. Law, "A new approach to the realization of a dual-band microstrip filter with very wide upper stopband"," *IEEE Trans. Microwave Theory Tech.*, vol. 56, no. 6, pp. 1461-1467, Jun. 2008.

[14] J.-T. Kuo and H.-P. Lin, "Dual-band bandpass filter with improved performance in extended upper rejection band," submitted to *IEEE Trans. Microwave Theory Tech.*, May 2008.

[15] G. L. Matthaei, L. Young and E. M. T. Jones, *Microwave Filters, Impedance-Matching Network, and Coupling Structures.* Norwood, MA: Artech House, 1980

[16] J. S. Hong and M. J. Lancaster, "Design of highly selective microstrip bandpass filters with a single pair of attenuation poles at finite frequencies," *IEEE Trans. Microwave Theory and Tech.*, vol.48, No. 7, July 2000, pp. 1098-1107.

[17] J. S. Wong, "Microstrip tapped-line filter design," *IEEE Trans. Microw. Theory Tech.*, vol. MTT-27, pp. 44–50, Jan. 1979

[18] G. L. Mattaei, L. Young and E. M. T. Jones, *Microwave Filters, Impedance-Matching Network, and Coupling Structures*, Norwood MA: Artech House, 1980.

[19] D. M. Pozar, Microwave Engineering, 2nd ed. New York: Wiley, 1998.

[20] *IE3D Simulator*, Zeland Software Inc., Jan. 1997.